Journal of Volcanology and Geothermal Research 420 (2021) 107393

Contents lists available at ScienceDirect

Journal of Volcanology and Geothermal Research

journal homepage: www.elsevier.com/locate/jvolgeores

Determining physical and mechanical volcanic rock properties via reflectance spectroscopy

Lauren N. Schaefer [a,1], Gabor Kereszturi [b], Marlene Villeneuve [c,*], Ben Kennedy [a]

[a] Earth and Environment, University of Canterbury, Private Bag 4800, Christchurch 8140, New Zealand
[b] Volcanic Risk Solutions, School of Agriculture and Environment, Massey University, Private Bag 11 222, Palmerston North 4442, New Zealand
[c] Subsurface Engineering, Montanuniversität Leoben, A-8700 Leoben, Franz-Josef-Strasse 18, Austria

ARTICLE INFO

Article history:
Received 17 May 2021
Received in revised form 3 September 2021
Accepted 6 September 2021
Available online 9 September 2021

Keywords:
Transfer function
Andesite
Hydrothermal alteration
Weathering
Iron-bearing mineral phases
Clay
Short wave infrared
Visible spectrum
Reflectance spectroscopy

ABSTRACT

There are currently no reliable methods to determine rock physical and mechanical properties that are not labor or resource intensive, especially at the scale of volcanoes. Using mineralogical-physical-mechanical relationships, we suggest it is possible to derive rock properties from rapid, non-invasive reflectance spectroscopy measurements. To demonstrate this potential, we correlate the physical and mechanical properties of variously altered andesitic volcanic rocks to laboratory reflectance spectroscopy using statistical analysis. Several rock properties, including density, connected porosity, strength, magnetic susceptibility, and elasticity, correlate with reflectance spectroscopy in both the visible and short-wave infrared parts of the electromagnetic spectrum. We attribute these correlations to the presence and degradation (i.e. weathering or hydrothermal alteration) of iron-bearing minerals such as pyroxene, magnetite, and pyrite, which reflect changes to both rock properties and reflectance spectroscopy measurements. Results support the use of transfer functions to estimate rock properties directly from reflectance spectroscopy. Ultimately, aerial or satellite imaging spectroscopy could be used to create geotechnical maps at volcano scale.

© 2021 The Author(s). Published by Elsevier B.V. This is an open access article under the CC BY license (http://creativecommons.org/licenses/by/4.0/).

1. Introduction

The geotechnical and geomechanical characterization of rock is critical for mapping and analyzing land use and land cover systems, ranging from mineral resources to hazard susceptibility. In volcanic environments, the characterization of volcanic material is critical for numerical modeling of instability and mass flows, interpreting geophysical signals of volcano unrest (e.g. volcano-seismic or geodetic), and assessing volcanic hazards (e.g. Apuani et al., 2005; Heap et al., 2020; Heap and Violay, 2021; Lavallée and Kendrick, 2021). Determining mechanical properties, such as strength and elasticity, is resource- and time-consuming for sample collection, preparation and lab testing, and requires specialized laboratory equipment. Additionally, inherent heterogeneities in volcanic systems and rock variability ranging from the micro to macro scale make representative sampling and volcano-wide assessment difficult because of the scale and challenging terrain of most volcanoes. Many laboratory methods and models cannot capture the characteristics of large rock masses (e.g. the influence of fractures on permeability (Heap and Kennedy, 2016) or elasticity (Heap et al., 2020)), emphasizing the need to develop methods that can be translated to field-scale operations.

Infrared reflectance spectroscopy, or hyperspectral scanning, measures the amount of energy an object reflects at hundreds of narrow and contiguous spectral bands, typically in the visible (VIS; 380–720 nm), near-infrared (NIR; 720–1000 nm), and shortwave infrared (SWIR; 1000–2500 nm) wavelengths. Because each material reflects and absorbs electromagnetic radiation differently due to varying composition and texture, this technique can identify physical and chemical properties of materials quickly and noninvasively using characteristic absorption and reflection features across the electromagnetic spectrum (van der Meer, 2018). In volcanic and geothermal environments, spectroscopy is often used to identify indicator minerals for weathering or hydrothermal alteration (e.g. Simpson and Rae, 2018; Rodriguez-Gomez et al., 2021; Savitri et al., 2021). These indicator minerals can form under oxidizing conditions as a weathering product of iron-bearing minerals, such as goethite and jarosite (Zimbelman et al., 2005), or under hydrothermal conditions, which produces alunite, gypsum, anhydrite, muscovite, biotite, epidote, carbonates, and phyllosilicate clay minerals (Aslett et al., 2018; Kereszturi et al., 2018; Gabrieli et al., 2019). We suggest it is possible to derive physical and mechanical properties from reflectance spectroscopy using mineralogical-

* Corresponding author.
E-mail address: marlene.villeneuve@unileoben.ac.at (M. Villeneuve).
[1] U.S. Geological Survey, 1711 Illinois St., Golden, CO, 80401, USA.

https://doi.org/10.1016/j.jvolgeores.2021.107393
0377-0273/© 2021 The Author(s). Published by Elsevier B.V. This is an open access article under the CC BY license (http://creativecommons.org/licenses/by/4.0/).

physical-mechanical relationships associated with the pervasiveness of weathering and hydrothermal alteration (e.g. Pola et al., 2012; Schaefer et al., 2020).

This study presents the first library of rock physical and mechanical property relationships to reflectance spectroscopy. The physical and mechanical properties of variably weathered and hydrothermally altered lava, autoclastic breccia, and pyroclastic andesitic volcanic rock samples are statistically correlated to their VIS-SWIR reflectance measurements to determine the predictive capability at different electromagnetic wavelengths. Bridging rock physical and mechanical testing with rapid proxy information such as spectroscopy, could transform how we predict the spatial heterogeneity of geotechnical properties of volcanic material. Using transfer functions, which are equations that relate one parameter to another (or others) using regression-based statistics, spectroscopy-based methods can provide new access to picture geomechanical properties at the scale of a volcano.

2. Methodology

This study used two sets of samples from Mt. Ruapehu volcano in New Zealand, including (1) 23 samples of lava, autoclastic breccia, and pyroclastic material as described in Schaefer et al. (2020), and (2) 6 representative samples of lava and autoclastic breccia from geotechnical units described in Mordensky et al. (2018). Samples follow the same naming convention as these previous studies. Mt. Ruapehu is a complex andesitic stratovolcano with an active hydrothermal system underneath the summit vent that hosts a crater lake (Fig. 1a). Additional older hydrothermal systems are variably exposed at the surface around the summit plateau (Kereszturi et al., 2020; Miller et al., 2020), resulting in a variety of fresh, weathered, and hydrothermally altered material (Fig. 1b), which is reflected in the sample suite chosen for this study (Fig. 1c). The physical and mechanical properties of the samples, including dry bulk density, connected porosity (henceforth referred to simply as "porosity"), magnetic susceptibility, matrix permeability (henceforth referred to simply as "permeability"), compressional (P-wave velocity or Vp) and shear wave (S-wave velocity or Vs) seismic velocity, uniaxial compressive strength (UCS), static Young's modulus, friction angle, cohesion, and the Hoek-Brown material constant for intact rock m_i were characterized for dry samples using the laboratory methods described in Mordensky et al. (2018) and Schaefer et al. (2020). The Hoek-Brown material constant for intact rock m_i (Eberhardt, 2012) is a parameter derived from triaxial compressive testing, which, along with the UCS, is used to derive the Hoek-Brown failure criterion for rock strength, in much the same way that friction angle and cohesion are used to derive the Mohr-Coulomb failure criterion.

Mineralogical composition for the Schaefer et al. (2020) dataset was determined via infrared spectroscopy and scanning electron microscopy (SEM) with energy-dispersive X-ray spectroscopy (EDS) (see

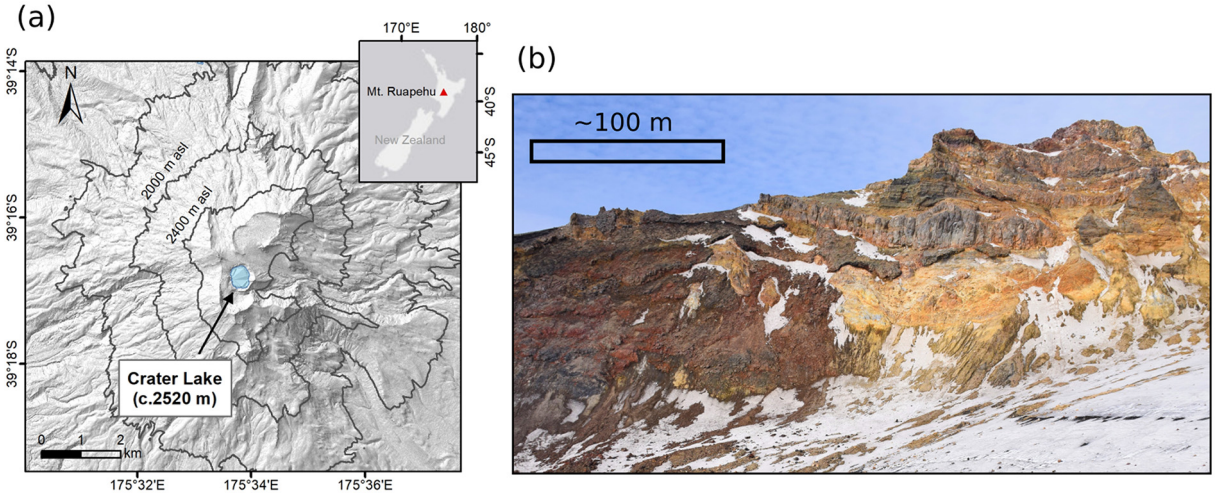

(c)

rock type	lava	autoclastic breccia	lava	autoclastic breccia	autoclastic breccia
weathering/ alteration type	surface weathering	fresh	supergene	surface weathering	steam-heated
weathering/ alteration extent	minor	none	moderate	pervasive	pervasive
porosity (%)	5.6	22.5	17.4	24.6	42.7
UCS (MPa)	258	40.5	66.2	26.8	12.7

Fig. 1. Location of Mt. Ruapehu and examples of a highly heterogeneous outcrop and rock samples. (a) Location of Mt. Ruapehu on the North Island of New Zealand (inset) and topographic map highlighting the Crater Lake. (b) Outcrop on the south rim of Mt. Ruapehu's summit plateau with varying degrees of weathering and hydrothermal alteration. (c) Rock samples with varying weathering or hydrothermal alteration types and pervasiveness, porosities, and uniaxial compressive strengths (UCS).

details in Mordensky et al., 2018; Kereszturi et al., 2020). In Schaefer et al. (2020), samples were categorized into four mineral assemblages defined by their alteration indicator minerals, occurrence, and origin, as follows: (1) Fresh, consisting of primary mineralogy such as pyroxene, plagioclase, and titanomagnetite; (2) Surface weathering, consisting of primary and chemically weathered and oxidized minerals, including Fe-oxides (hematite) and minor smectites typically occurring in a weathered rim; (3) Supergene, argillic alteration that develops at <40 °C through long-term weathering and oxidation of ferrous and minor sulfide-bearing rocks in atmospheric conditions, which includes phyllosilicates, jarosite, and Fe-oxides; (4) Steam-heated, intermediate and advanced argillic alteration that develops at <120 °C near the water table and in the shallowest epithermal environment, including, quartz, pyrite, Fe oxides (goethite), phyllosilicates, sulfur, and occasional jarosite and alunite (Table S1).

In addition to various mineral assemblages, samples also showed variations in alteration pervasiveness. Thus, samples were also categorized into four groups based on the extent of weathering/alteration, including "none" (fresh material), "minor" (typically only the exterior/crust of the sample is weathered or altered), "moderate" (weathering or alteration is variably present in the groundmass and crystals), and "pervasive" (weathering or alteration is strongly present in groundmass and crystals) (Table S1). Samples from Mordensky et al. (2018) were assigned weathering and hydrothermal alteration categories based on descriptions in that publication.

Averaged physical and mechanical properties for each rock, along with descriptions of the major alteration mineral phases and the extent of weathering or hydrothermal alteration are given in Supplementary Table S1.

Spectral reflectance, defined as a ratio between the total incoming and the reflected light, of both the natural rock surface and of a rock powder for each sample were measured using an ASD 4 FieldSpec High Resolution spectroradiometer. While drilled cores were used to determine physical and mechanical properties of the rock samples, the artificial smoothness and shininess introduced during drilling resulted in inaccurate reflectance readings (e.g. noisy VIS spectrum). To ensure the bulk mineralogy of the rock was well represented, spot readings were taken of freshly chipped surfaces of the drilled cores and other rock pieces, for a total of 3–5 measurements per sample. These measurements were averaged to produce one spectral reading per rock sample. Thus, we consider that the spectral readings of the rock samples are representative of the drilled and tested cores. Additionally, 5–6 g powdered samples were made of each sample (core or rock pieces) using a benchtop ring mill until the samples reached a homogenous grain size (typically ≤500 μm). Three spectral measurements were made of each powder and averaged to produce one spectral reading per sample.

Spearman's rank correlation coefficient (SCC), also referred to as Spearman's ρ, was used to correlate spectral reflectance at a wavelength, λ, (X_λ) with each of the physical or mechanical properties (Y). Spearman's rank correlation coefficient is a measure of the monotonic correlation between two variables as:

$$\text{SCCwavelength}\ (\rho) = \frac{cov(X_\lambda, Y)}{\sigma_X \sigma_Y} \quad (1)$$

where the covariance is Σ(x - mean(X_λ)) × (y - mean(Y)) × 1/(n-1), and the σ_X and σ_Y are the standard deviation of the spectral and physical rock properties, respectively. The resulting value, Spearman's ρ value, varies between 1 and − 1, where '1' indicates a total positive correlation, '0' indicates no correlation, and '−1' is a total negative correlation.

The dataset was explored by plotting the Spearman's rank correlation coefficients for each physical and mechanical property at each tested wavelength (Fig. 2). These were compared to the normalized reflectance spectra of key minerals to link reflectance features to geochemical components (Fig. 2). Spectral reflectance was normalized to a common baseline to make absorption features easier to compare, which transforms the data to be between 0 (absorption feature) and 1 (baseline or background). Absorption features (dips in the spectra) are unique for each mineral (Fig. 2).

3. Spectroscopy-rock property correlations

The normalized spectral reflectance curve of several common minerals found in the rock samples, including goethite (iron oxide weathering product of iron-bearing minerals such as pyrite or (titano-) magnetite), jarosite (weathering product of pyrite), kaolinite and montmorillonite (weathering or hydrothermal alteration of aluminosilicate minerals), and enstatite and augite (pyroxene that forms as part of the primary magmatic mineralogy). Each of these minerals highlights the unique absorption features (dips in the spectra) for each of these minerals at various wavelengths (Fig. 2a). The spectral reflectance values and associated correlations are only shown for rock, however powdered sample correlations are available in Supplementary Material (Fig. S1). Correlations between rock properties and rock spectral measurements at a given wavelength between 350 and 2500 nm are shown in Fig. 2b, where the strength of the correlation (Spearman's ρ value) can generally be interpreted as fair to poor under (+/−) 0.40, increasing to a perfect correlation at (+/−) 1.0 (Akoglu, 2018). These correlation coefficients were used to screen for the highest correlation zones, which were then visually inspected and interpreted following Schober et al. (2018). Measurements above 2400 nm are generally noisy due to instrument noise, and thus are not considered reliable relationship indicators. Additionally, the spectral curves of each rock and powder sample are given in the Supplementary Material (Figs. S2 and S3).

3.1. Results

Spearman's ρ values for all tested material properties at the highest correlating wavelength, ranked from strongest to weakest correlation (positive or negative) at the given wavelength are given in Table 1 for rocks and powders. The strength of the correlation can be interpreted as follows: (−)0.40 to (−)0.59 is a "moderate" correlation, (−)0.60 to (−)0.79 is a "strong" correlation, and (−)0.80 to (−)1.0 is a "very strong" correlation. Most material properties have "strong" correlation, while the remaining have "moderate" correlation. The maximum Spearman's ρ values, and the wavelengths at which they occur, differ depending on whether the reflectance is from a rock surface or a powder.

Moderate to strong (monotonic) correlations exist in the VIS and SWIR regions for all material properties (Fig. 2b). Between 365 and 390 nm, magnetic susceptibility and density both have Spearman's ρ values over 0.6, while porosity, permeability, UCS, static Young's modulus, friction angle, cohesion, P-wave velocity, and S-wave velocity have Spearman's ρ values between 0.4 and 0.59. Between 2250 and 2420 nm, static Young's modulus, friction angle, UCS, porosity, and magnetic susceptibility have Spearman's ρ values over 0.6, while permeability, density, P-wave velocity, S-wave velocity, mi, and cohesion have Spearman's ρ values between 0.4 and 0.59. Correlations in the NIR (750–1400 nm) and beginning of the SWIR (1400–2000 nm) are generally poor (< 0.4).

The process of powdering can both normalize for grain size variations and the proportion of original to altered minerals (e.g. weathering rim vs. pervasively altered samples), resulting in more representative measurements of bulk rock spectroscopy. In our dataset, powdered and rock sample spectra follow very similar correlation patterns between 350 and 2500 nm (Supplementary Fig. S1). These results suggest that field measurements on rock can still detect expected mineralogical trends and create reliable datasets without the need for more resource and time-intensive sample preparation. We additionally caution that our laboratory measurements were made on oven-dried samples, and that

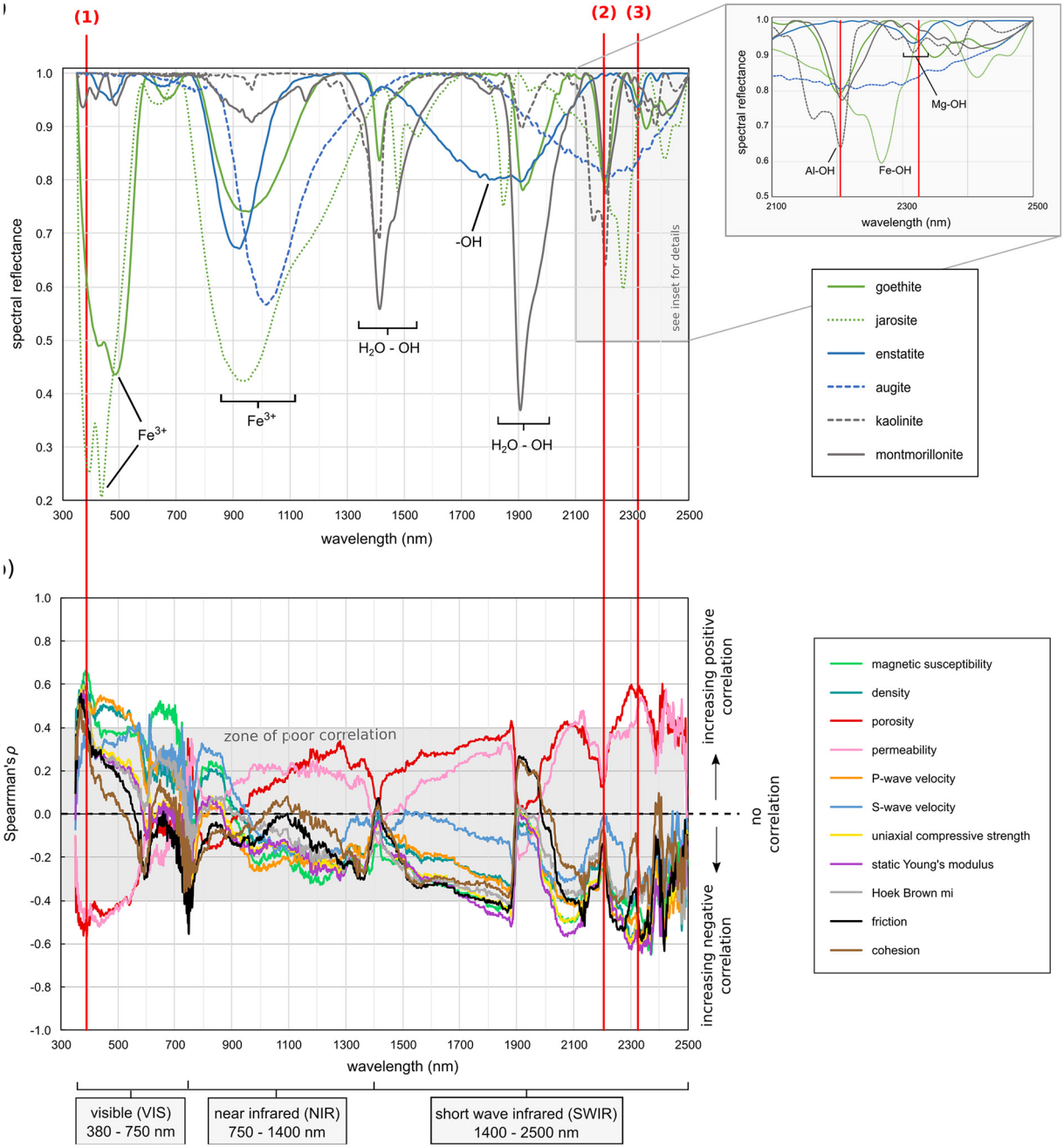

Fig. 2. (a) The normalized spectral reflectance curve of common minerals found in the sample suite. Reflectance values of '1' indicate baseline or background values, and values of '0' indicate full absorption of light at the given wavelength. Absorption features (dips in the spectra) are unique for each mineral. (b) Spearman's ρ value between physical and mechanical properties and spectral reflectance at a given wavelength. Red vertical lines and associated numbers highlight wavelengths discussed in text and Fig. 3.

water content in the field can significantly impact both material properties (Karakul and Ulusay, 2013) and spectroscopy measurements (Kereszturi et al., 2018). Furthermore, many rocks tend to have weathered crusts but unweathered interiors (e.g. Mordensky et al., 2019; Kereszturi et al., 2020), which could incorrectly categorize rocks into more pervasively weathered or altered categories. Thus, we suggest that field measurements are made on a freshly chipped surface if possible.

3.2. Visible region trends

In the visible (VIS) region, most properties show moderate to strong correlations around 365–390 nm (red vertical line '1' in Fig. 2). This relates to absorption features of Fe-rich sulfates (e.g. jarosite) and Fe-rich oxides (e.g. goethite) (Fig. 2a), common weathering and alteration minerals in active andesitic volcanic environments (Schwertmann and Murad, 1983; Noack et al., 1993; Bishop and Murad, 2005; Kereszturi et al., 2020). As rocks weather and alter to form these minerals, several physical and mechanical properties are also impacted. For example, fresh rocks with more titanomagnetite content have higher values of magnetic susceptibility. As titanomagnetite is dissolved to form pyrite, and subsequently, goethite under supergene conditions, the magnetism of the rock is reduced (Miller et al., 2020). Fig. 3a highlights this process, where rocks with more pervasive alteration have lower magnetic susceptibility and lower reflectance values (or larger absorption features) at 390 nm, indicating a higher percentage of goethite or jarosite.

Table 1
Material property and its associated Spearman's ρ value at the highest correlating wavelength for both rock and powder samples, ranked from strongest to weakest correlation (positive or negative) at the given wavelength.

Rock		
Property	Spearman's ρ	Wavelength (nm)
Magnetic susceptibility	0.67	389
Static Young's modulus	−0.65	2370
Friction angle	−0.63	2418
Density	0.61	380
UCS	−0.61	2339
Porosity	0.60	2411
Permeability	0.58	2423
Vp	−0.57	2423
m_i	0.52	391
Cohesion	0.51	367
Vs	0.46	611
Powder		
Property	Spearman's ρ	Wavelength (nm)
Cohesion	−0.74	2430
Friction angle	0.69	370
UCS	−0.64	2319
m_i	0.64	381
Static Young's modulus	0.61	379
Vp	0.60	380
Permeability	−0.59	470
Magnetic susceptibility	0.57	701
Porosity	−0.57	375
Density	0.56	380
Vs	0.46	573

Fig. 3a also shows that more pervasive alteration generally correlates to lower rock strength (measured as uniaxial compressive strength, UCS) and lower reflectance values (or larger absorption features) at 390 nm, which indicates a higher presence of Fe-oxides and sulfates. Surface weathering and hydrothermal alteration can replace the primary denser minerals (e.g. pyroxene, titanomagnetite) with less dense secondary minerals (e.g. goethite, jarosite), lowering rock strength (Siratovich et al., 2014; Wyering et al., 2014). Porosity also shows a strong trend with spectral reflectance values, alteration pervasiveness, and strength. This trend could be a function of initial porosity, where more porous material alters faster because of the larger amount of void space for fluids to move through the rock. Alternatively, this trend could result from higher alteration intensity, derived from dissolution of primary minerals to increase porosity and permeability (e.g. Cant et al., 2018a; Farquharson et al., 2019). A similar trend has been reported in soil studies, where an increase in Fe-oxides has been shown to positively correlate with porosity and negatively correlate with strength (e.g. Yildiz et al., 2018). Porosity and permeability show an inverse correlation with reflectance from the other material properties (Fig. 2) as both increase with increasing pore and crack space (e.g. Cant et al., 2018a), while strength, stiffness, density, and seismic wave velocities typically decrease with increasing pore and crack space (e.g. Heap and Violay, 2021).

3.3. Shortwave infrared region trends

Figs. 2 and 3b–c highlight wavelengths in the shortwave infrared (SWIR) region associated with poor (around 2200 nm, red line '2' in Figs. 2, 3b) and high (around 2325 nm, red line '3' in Figs. 2, 3c) material property-spectral reflectance correlations. Around 2200 nm, Spearman's ρ values for all material properties decrease significantly, which is also a region associated with typical absorption features due to -OH, Al-OH and Mg-OH bonds in clays and sulfates (e.g. kaolinite and montmorillonite). While an increase in weathering or alteration would intuitively correlate to a decrease in strength, several authors have found it can have varying influences on material properties. Acid-sulphate alteration can precipitate clay, silicate and other minerals into pores and cracks, reducing porosity and permeability and increasing strength (Heap et al., 2019b; Kennedy et al., 2020). Alternatively, acid dissolution of primary minerals can widen pore throat apertures (e.g. Farquharson et al., 2019) and microcracks (e.g. Mordensky et al., 2018), leading to an increase in porosity and permeability and decrease in strength. Thus, we attribute the poor correlations to the varying influence of clay alteration on material with varying primary mineralogy and density/porosity.

At 2325 nm, most material physical and mechanical properties show moderate to strong correlations with spectral reflectance values (Fig. 3c). This wavelength is near absorption features of pyroxene minerals, specifically, Fe and Mg absorption features of enstatite and augite, both of which are abundant primary groups at Mt. Ruapehu (Price et al., 2012). We interpret the good correlation in this region to be associated with the presence and subsequent degradation of pyroxenes through weathering or alteration (Noack et al., 1993). This is highlighted in Fig. 3c, where more extensively altered material has lower strength and higher spectral reflectance (or lower absorption features) at 2325 nm, indicating a lower abundance of fresh pyroxenes. Like trends in the VIS, unaltered material shows a large spread in spectral reflectance values, likely due to variations in the original pyroxene content of these rocks.

4. Discussion

The moderate to strong correlations of several rock properties to lab-based spectroscopy are encouraging for the future development and use of transfer functions to determine geotechnical properties from remote sensing data. This could reduce the need for field and laboratory physical and mechanical testing and improve the spatial extrapolation of existing measurements. While properties with higher Spearman ρ values are more reliable for creating transfer functions (Fig. 2; Table 1), mechanical studies of volcanic rocks have established several relationships between physical and mechanical properties that could be used to produce full geotechnical profiles. For example, porosity has repeatedly been shown to have a first order control on other mechanical and physical properties, with increasing porosity resulting in an increase in permeability and decrease in UCS, Young's modulus, Vp, Poisson's ratio, and mi (e.g. Al-Harthi et al., 1999; Pola et al., 2012; Heap et al., 2014, Heap et al., 2014b, Heap et al., 2015, Heap et al., 2019a; Schaefer et al., 2015; Cant et al., 2018a; Coats et al., 2018b), and is a clear candidate as a basis for transfer functions. However, a strong relationship does not exist between porosity and magnetic susceptibility, nor with strength for rocks with <10% porosity (Fig. 3). This suggests that mineralogical and physical properties both influence the correlation of rock properties to spectroscopy and need to be considered when developing transfer functions.

Both rock properties and spectral reflectance values show good correlation to the pervasiveness or extent of alteration apart from unaltered rock, which has a large spread in both rock properties and reflectance values. While rocks with more weathering or hydrothermal alteration tend to have lower P-wave velocities, higher porosity, higher permeability, and lower UCS than their unaltered counterparts, this is not always the case (e.g. Mordensky et al., 2018) and these properties can be controlled by their primary mineralogy and porosity/density in unaltered rocks. For example, the porosity of an unaltered autoclastic breccia can be over 35%, while unaltered lava tends to be under 10% (Supplementary Table 1; Schaefer et al., 2020). Thus, it may be difficult to create transfer functions to directly correlate alteration extent to spectral reflectance. Future work could use quantified alteration indicators to investigate this potential (e.g. the alteration % used in Heap and Violay, 2021).

While this study is encouraging for developing spectroscopy-material property correlations at larger scales, there are also limitations. First, rocks from a single volcano with a single primary lithology (andesite) were used, and therefore we do not provide any transfer functions

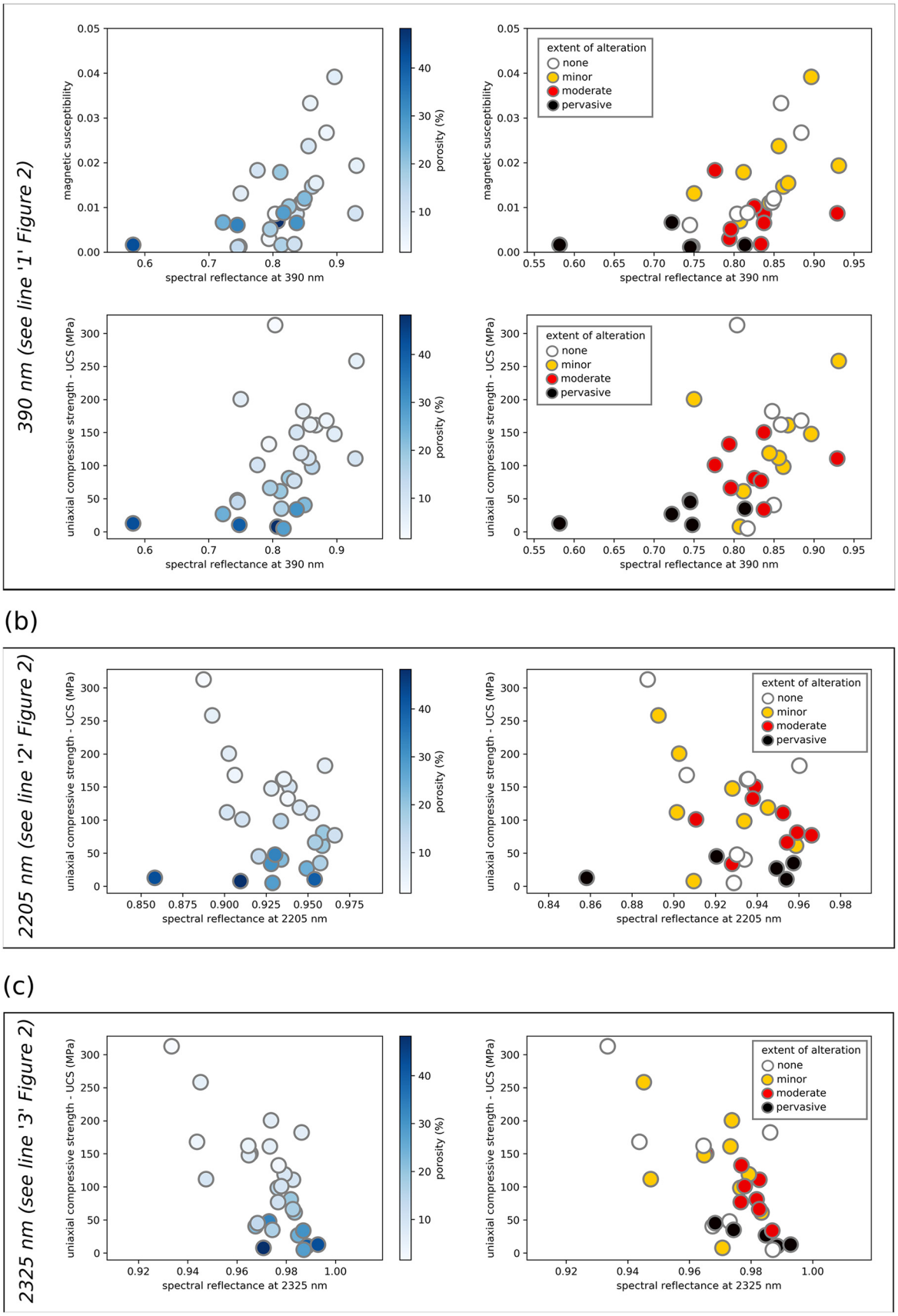

Fig. 3. Relationships between rock physical or mechanical properties and their spectral reflectance at a given wavelength, with porosity (left column) or extent of alteration (right column) for each sample highlighted. (a) Correlations of magnetic susceptibility (top row) and UCS (bottom row) at 390 nm, referenced by red vertical line '1' in Fig. 2. (b) Correlation of UCS at 2205 nm, referenced by red vertical line '2' in Fig. 2. (c) Correlation of UCS at 2325 nm, referenced by red vertical line '3' in Fig. 2.

based on our results. The development of robust transfer functions based on volcanic rocks from a variety of volcanoes in a variety of volcanic environments constitutes continuing research. Second, spectroscopy imaging can only reveal surface information, however material properties change at depth with variations in temperatures, pressures, fluids, and the types and pervasiveness of alteration (e.g. Siratovich et al., 2016). Volcano edifice-scale parameters, such as seismic velocity, strength, stiffness and permeability, also strongly depend on factors such as temperature and large-scale fracturing, which cannot be accounted for by laboratory-scale intact rock properties alone (Heap and Kennedy, 2016; Heap et al., 2020). Thus, we caution that inherent heterogeneities in volcanic systems may require site-specific calibration, and that there are several considerations when upscaling laboratory-based intact rock properties to field-scale, or translating surface rock properties to depth. Future studies linking lab- and field-scale measurements are needed to refine these relationships. Finally, when upscaling from lab-based hyperspectral to air/space-based remote sensing atmospheric interference and rock surfaces obscured by soil, tephra, and vegetation will affect the quality of the spectral signals. The gap between lab- and air/space-scale will likely require infilling with meso-scale measurements, for example using drone-based sensors.

The increase in global coverage of spectroscopy data is promising for applications such as geophysical and geodetic measurements, geologic interpretations, and modeling that benefit from knowing the spatial variability of material properties. Currently, global coverage is available at a lower resolution (e.g. ASTER satellite with 15 spectral bands and 15–90 m spatial resolution), but the availability of higher resolution hyperspectral data continues to increase, such as the PRISMA (30 m) mission (Cogliati et al., 2021) or EnMAP (30 m) mission (Guanter et al., 2015). Higher resolution spatial mapping of material properties can highlight the influence of contrasting material parameters on, for example, landslide susceptibility (Bunn et al., 2020), which tends to be masked when using large-scale, uniform classifications (Hwang et al., 2015). The good correlation of material properties with the visible spectrum also suggests that current high-spectral resolution multispectral data could be used to extrapolate material properties.

Our data also show that currently active and older magmatic or hydrothermal systems can be distinguished based on the presence of Fe + signatures in the visible light spectrum, shedding light on the evolution of volcanic systems and identifying hazards (e.g. hydrothermal alteration-driven flank collapse). While this study has been conducted on an andesitic volcano, Zhou and Wang (2017) showed that fresh and altered spectra are different for a variety of volcanic and non-volcanic rock types. Therefore, the opportunity exists to calibrate this approach for other environments. Thus, we encourage adding spectroscopy measurements to the suite of commonly collected petro-characterizations in the laboratory or field.

5. Conclusion

Several physical and mechanical laboratory intact rock properties of a suite of variably altered andesitic volcanic lavas, autoclastic breccias, and pyroclastic rocks from Mt. Ruapehu volcano in New Zealand were correlated to laboratory reflectance spectroscopy measurements using the Spearman correlation coefficient, revealing good relationships. Our results show that iron-bearing mineral phases are sensitive to weathering and hydrothermal alteration due to primary mineral degradation and dissolution to secondary minerals (e.g. pyroxene and titanomagnetite to goethite and jarosite). Thus, they are good indicators for correlations between a rock's physical and mechanical properties and their spectral reflectance value in both the visible and shortwave infrared regions of the electromagnetic spectrum. In contrast, we find that areas of the electromagnetic spectrum of typical absorption features of clays (e.g. kaolinite, montmorillonite) do not show good correlation to physical and mechanical properties due to the varying influence clay alteration can have on rock properties.

While laboratory or field measurements should be made when possible, spectroscopy could provide a first-order estimate of rock properties when little to no information is available and allow for the spatial interpolation of material properties between sample locations. These laboratory correlations are also a proof of concept for predicting rock mechanical properties over large spatial scales using airborne or satellite hyperspectral data (e.g. PRISMA or EnMAP), with applications to both Earth and planetary studies. We suggest that field spectrometers could be used as a portable tool alongside other in-situ measurements or in the lab as a relative measure of several physical and mechanical properties, which can help to develop spectroscopy-material property relationships in volcanic and non-volcanic environments.

Data availability

Datasets for this research are included in this paper (and its supplementary information files), and through Mordensky et al. (2018), Kereszturi et al. (2020), and Schaefer et al. (2020).

Declaration of Competing Interest

The authors declare that they have no known competing financial interests or personal relationships that could have appeared to influence the work reported in this paper.

Acknowledgements

This research was supported by the New Zealand Ministry of Business, Innovation & Employment's Natural Hazards Research Platform for the project “Too big to fail? – A multidisciplinary approach to predict collapse and debris flow hazards from Mt. Ruapehu,” grant number 3000031404. The authors declare no conflicts of interest.

Appendix A. Supplementary data

Supplementary data to this article can be found online at https://doi.org/10.1016/j.jvolgeores.2021.107393.

References

Akoglu, H., 2018. User's guide to correlation coefficients. Turk. J. Emerg. Med. 18, 91–93.
Al-Harthi, A.A., Al-Amri, R.M., Shehata, W.M., 1999. The Porosity and Engineering Properties of Vesicular Basalt in Saudi Arabia. Engineering Geology https://doi.org/10.1016/S0013-7952(99)00050-2.
Apuani, T., Corazzato, C., Cancelli, A., Tibaldi, A., 2005. Stability of a collapsing volcano (Stromboli, Italy): Limit equilibrium analysis and numerical modelling. J. Volcanol. Geotherm. Res. 144, 191–210. https://doi.org/10.1016/j.jvolgeores.2004.11.028.
Aslett, Z., Taranik, J.V., Riley, D.N., 2018. Mapping rock forming minerals at Boundary Canyon, Death Valley National Park, California, using aerial SEBASS thermal infrared hyperspectral image data. Int. J. Appl. Earth Obs. Geoinf. https://doi.org/10.1016/j.jag.2017.08.001.
Bishop, J.L., Murad, E., 2005. The visible and infrared spectral properties of jarosite and alunite. Am. Mineral. 90, 1100–1107.
Bunn, M., Leshchinsky, B., Olsen, M.J., 2020. Geologic trends in Shear strength properties inferred through three-dimensional back-analysis of landslide inventories. J. Geophys. Res. Earth Surf. 125. https://doi.org/10.1029/2019JF005461 e2019JF005461.
Cant, J.L., Siratovich, P.A., Cole, J.W., Villeneuve, M.C., Kennedy, B.M., 2018a. Matrix Permeability of Reservoir Rocks, Ngatamariki Geothermal Field, Taupo Volcanic Zone. Geothermal Energy, New Zealand https://doi.org/10.1186/s40517-017-0088-6.
Coats, R., Kendrick, J.E., Wallace, P.A., Miwa, T., Hornby, A.J., Ashworth, J.D., Matsushima, T., Lavallée, Y., 2018b. Failure criteria for porous dome rocks and lavas: a study of Mt. Unzen, Japan. Solid Earth 9, 1299–1328. https://doi.org/10.5281/zenodo.1287237.
Cogliati, S., et al., 2021. The PRISMA imaging spectroscopy mission: overview and first performance analysis. Remote Sens. Environ. 262, 112499.
Eberhardt, E., 2012. The Hoek–Brown failure criterion. Rock Mechanics and Rock Engineering 45 (6), 981–988. https://doi.org/10.1007/s00603-012-0276-4.
Farquharson, J.I., Wild, B., Kushnir, A.R.L., Heap, M.J., Baud, P., Kennedy, B., 2019. Acid-induced dissolution of Andesite: evolution of permeability and strength. J. Geophys. Res. Solid Earth https://doi.org/10.1029/2018JB016130.
Gabrieli, A., Wright, R., Porter, J.N., Lucey, P.G., Honnibal, C., 2019. Applications of Quantitative Thermal Infrared Hyperspectral Imaging (8–14 μm): Measuring Volcanic SO2 Mass Flux and Determining Plume Transport Velocity Using a Single Sensor: Bulletin of Volcanology. https://doi.org/10.1007/s00445-019-1305-x.

Guanter, L., et al., 2015. The EnMAP spaceborne imaging spectroscopy mission for earth observation. Remote Sens. 7, 8830–8857.
Heap, M.J., Kennedy, B.M., 2016. Exploring the scale-dependent permeability of fractured andesite. Earth Planet. Sci. Lett. 447, 139–150.
Heap, M.J., Lavallée, Y., Petrakova, L., Baud, P., Reuschle, T., Varley, N.R., Dingwell, D.B., 2014. Microstructural controls on the physical and mechanical properties of edifice-forming andesites at Volcán de Colima, Mexico. J. Geophys. Res. Solid Earth 119, 2925–2963. https://doi.org/10.1002/2013JB010521.
Heap, M.J., Violay, M.E., 2021. The mechanical behaviour and failure modes of volcanic rocks: a review. Bulletin of Volcanology 83 (5), 1–47. https://doi.org/10.1007/s00445-021-01447-2.
Heap, M.J., Xu, T., Chen, C. Feng, 2014b. The influence of porosity and vesicle size on the brittle strength of volcanic rocks and magma. Bull. Volcanol. https://doi.org/10.1007/s00445-014-0856-0.
Heap, M.J., Farquharson, J.I., Wadsworth, F.B., Kolzenburg, S., Russell, J.K., 2015. Timescales for permeability reduction and strength recovery in densifying magma. Earth Planet. Sci. Lett. https://doi.org/10.1016/j.epsl.2015.07.053.
Heap, M.J., Gravley, D.M., Kennedy, B.M., Gilg, H.A., Bertolett, E., Barker, S.L.L., 2019a. Quantifying the role of hydrothermal alteration in creating geothermal and epithermal mineral resources: the ohakuri ignimbrite (Taupo Volcanic Zone, New Zealand). J. Volcanol. Geotherm. Res., 106703 https://doi.org/10.1016/j.jvolgeores.2019.106703.
Heap, M.J., Troll, V.R., Kushnir, A.R.L., Gilg, H.A., Collinson, A.S.D., Deegan, F.M., Darmawan, H., Seraphine, N., Neuberg, J., Walter, T.R., 2019b. Hydrothermal alteration of andesitic lava domes can lead to explosive volcanic behaviour. Nat. Commun. https://doi.org/10.1038/s41467-019-13102-8.
Heap, M.J., Villeneuve, M., Albino, F., Farquharson, J.I., Brothelande, E., Amelung, F., Got, J.L., Baud, P., 2020. Towards more realistic values of elastic moduli for volcano modelling. J. Volcanol. Geotherm. Res. https://doi.org/10.1016/j.jvolgeores.2019.106684.
Hwang, T., Band, L.E., Hales, T.C., Miniat, C.F., Vose, J.M., Bolstad, P.V., Miles, B., Price, K., 2015. Simulating vegetation controls on hurricane-induced shallow landslides with a distributed ecohydrological model. J. Geophys. Res. Biogeosci. https://doi.org/10.1002/2014JG002824.
Karakul, H., Ulusay, R., 2013. Empirical correlations for predicting strength properties of rocks from P-wave velocity under different degrees of saturation. Rock Mech. Rock. Eng. 46, 981–999.
Kennedy, B.M., Farquhar, A., Hilderman, R., Villeneuve, M.C., Heap, M.J., Mordensky, S., Kilgour, G., Jolly, A., Christenson, B., Reuschlé, T., 2020. Pressure controlled permeability in a conduit filled with fractured hydrothermal Breccia reconstructed from ballistics from Whakaari (White island). New Zealand: Geosciences 10, 138. https://doi.org/10.3390/geosciences10040138.
Kereszturi, G., Schaefer, L.N., Schleiffarth, W.K., Procter, J., Pullanagari, R.R., Mead, S., Kennedy, B., 2018. Integrating airborne hyperspectral imagery and LiDAR for volcano mapping and monitoring through image classification. Int. J. Appl. Earth Obs. Geoinf. https://doi.org/10.1016/j.jag.2018.07.006.
Kereszturi, G., Schaefer, L.N., Miller, C., Mead, S., 2020. Hydrothermal alteration on composite volcanoes -mineralogy, hyperspectral imaging and aeromagnetic study of Mt Ruapehu, New Zealand. Geochem. Geophys. Geosyst. https://doi.org/10.1029/2020GC009270.
Lavallée, Y., Kendrick, J.E., 2021. A Review of the Physical and Mechanical Properties of Volcanic Rocks and Magmas in the Brittle and Ductile Regimes: Forecasting and Planning for Volcanic Hazards, Risks, and Disasters. pp. 153–238.
Miller, C., Schaefer, L.N., Kereszturi, G., Fournier, D., 2020. Three dimensional mapping of Mt Ruapehu volcano, New Zealand, from aeromagnetic data inversion and hyperspectral imaging. J. Geophys. Res. Solid Earth 125. https://doi.org/10.1029/2019JB018247.
Mordensky, S.P., Villeneuve, M.C., Kennedy, B.M., Heap, M.J., Gravley, D.M., Farquharson, J.I., Reuschlé, T., 2018. Physical and mechanical property relationships of a shallow intrusion and volcanic host rock, Pinnacle Ridge, Mt. Ruapehu, New Zealand. J. Volcanol. Geotherm. Res. https://doi.org/10.1016/j.jvolgeores.2018.05.020.
Mordensky, S.P., Heap, M.J., Kennedy, B.M., Gilg, H.A., Villeneuve, M.C., Farquharson, J.I., Gravley, D.M., 2019. Influence of alteration on the mechanical behaviour and failure mode of andesite: implications for shallow seismicity and volcano monitoring. Bull. Volcanol. https://doi.org/10.1007/s00445-019-1306-9.
Noack, Y., Colin, F., Nahon, D., Delvigne, J., Michaux, L., 1993. Secondary-mineral formation during natural weathering of pyroxene; review and thermodynamic approach. Am. J. Sci. 293, 111–134.
Pola, A., Crosta, G., Fusi, N., Barberini, V., Norini, G., 2012. Influence of Alteration on Physical Properties of Volcanic Rocks: Tectonophysics. https://doi.org/10.1016/j.tecto.2012.07.017.
Price, R.C., Gamble, J.A., Smith, I.E.M., Maas, R., Waight, T., Stewart, R.B., Woodhead, J., 2012. The anatomy of an andesite volcano: a time-stratigraphic study of andesite petrogenesis and crustal evolution at Ruapehu Volcano, New Zealand. J. Petrol. https://doi.org/10.1093/petrology/egs050.
Rodriguez-Gomez, C., Kereszturi, G., Reeves, R., Rae, A., Pullanagari, R., Jeyakumar, P., Procter, J., 2021. Lithological mapping of Waiotapu Geothermal Field (New Zealand) using hyperspectral and thermal remote sensing and ground exploration techniques. Geothermics 96, 102195.
Savitri, K.P., Hecker, C., van der Meer, F.D., Sidik, R.P., 2021. VNIR-SWIR infrared (imaging) spectroscopy for geothermal exploration: Current status and future directions. Geothermics 96, 102178.
Schaefer, L.N., Kendrick, J.E., Lavallée, Y., Oommen, T., Chigna, G., 2015. Geomechanical rock properties of a basaltic volcano. Front. Earth Sci. 3, 29. https://doi.org/10.3389/feart.2015.00029.
Schaefer, L., Kereszturi, G., Kennedy, B., Villeneuve, M., 2020. Characterizing lithological, weathering, and hydrothermal alteration influences on volcanic. Earth Space Sci Open Arch., 32 https://doi.org/10.1002/essoar.10504173.1.
Schober, P., Boer, C., Schwarte, L.A., 2018. Correlation coefficients: appropriate use and interpretation. Anesth. Analg. 126, 1763–1768.
Schwertmann, U., Murad, E., 1983. Effect of pH on the formation of goethite and hematite from ferrihydrite. Clay Clay Miner. https://doi.org/10.1346/CCMN.1983.0310405.
Simpson, M.P., Rae, A.J., 2018. Short-wave infrared (SWIR) reflectance spectrometric characterisation of clays from geothermal systems of the Taupō Volcanic Zone, New Zealand. Geothermics 73, 74–90.
Siratovich, P.A., Heap, M.J., Villenueve, M.C., Cole, J.W., Reuschlé, T., 2014. Physical property relationships of the Rotokawa Andesite, a significant geothermal reservoir rock in the Taupo Volcanic Zone, New Zealand. Geotherm. Energy https://doi.org/10.1186/s40517-014-0010-4.
Siratovich, P.A., Heap, M.J., Villeneuve, M.C., Cole, J.W., Kennedy, B.M., Davidson, J., Reuschlé, T., 2016. Mechanical Behaviour of the Rotokawa Andesites (New Zealand): Insight into Permeability Evolution and Stress-Induced Behaviour in an Actively Utilised Geothermal Reservoir: Geothermics. https://doi.org/10.1016/j.geothermics.2016.05.005.
van der Meer, F., 2018. Near-infrared laboratory spectroscopy of mineral chemistry: a review. Int. J. Appl. Earth Obs. Geoinf. https://doi.org/10.1016/j.jag.2017.10.004.
Wyering, L.D., Villeneuve, M.C., Wallis, I.C., Siratovich, P.A., Kennedy, B.M., Gravley, D.M., Cant, J.L., 2014. Mechanical and physical properties of hydrothermally altered rocks, Taupo Volcanic Zone, New Zealand. J. Volcanol. Geotherm. Res. 288, 76–93. https://doi.org/10.1016/j.jvolgeores.2014.10.008.
Yildiz, A., Graf, F., Rickli, C., Springman, S.M., 2018. Determination of the Shearing Behaviour of Root-Permeated Soils with a Large-Scale Direct Shear Apparatus: Catena. https://doi.org/10.1016/j.catena.2018.03.022.
Zhou, K.-F., Wang, S.-S., 2017. Spectral properties of weathered and fresh rock surfaces in the Xiemisitai metallogenic belt, NW Xinjiang, China. Open Geosci. 9, 322–339.
Zimbelman, D.R., Rye, R.O., Breit, G.N., 2005. Origin of Secondary Sulfate Minerals on Active Andesitic Stratovolcanoes: Chemical Geology. https://doi.org/10.1016/j.chemgeo.2004.06.056.